Molecular Therapy
Nucleic Acids
Original Article

Efficacy of Postnatal In Vivo Nonsense Suppression Therapy in a *Pax6* Mouse Model of Aniridia

Xia Wang,[1] Kevin Gregory-Evans,[1] Kishor M. Wasan,[2] Olena Sivak,[1] Xianghong Shan,[1] and Cheryl Y. Gregory-Evans[1]

[1]Department of Ophthalmology and Visual Sciences, University of British Columbia, Vancouver, BC V5Z 3N9, Canada; [2]College of Pharmacy and Nutrition, University of Saskatchewan, Saskatoon, SK S7N 5A2, Canada

Nonsense mutations leading to premature stop codons are common occurring in approximately 12% of all human genetic diseases. Thus, pharmacological nonsense mutation suppression strategies would be beneficial to a large number of patients if the drugs could be targeted to the affected tissues at the appropriate time. Here, we used nonsense suppression to manipulate Pax6 dosage at different developmental times in the eye of the small eye (*Pax6*$^{Sey/+}$; G194X) mouse model of aniridia. Efficacy was assessed by functional assays for visual capacity, including electroretinography and optokinetic tracking (OKT), in addition to histological and biochemical studies. Malformation defects in the *Pax6*$^{Sey/+}$ postnatal eye responded to topically delivered nonsense suppression in a dose- and time-dependent manner. Elevated levels of Mmp9, a direct downstream target of Pax6 in the cornea, were observed with the different treatment regimens. The lens capsule was particularly sensitive to Pax6 dosage, revealing a potential new role for Pax6 in lens capsule maintenance and development. The remarkable capacity of malformed ocular tissue to respond postnatally to Pax6 dosage in vivo demonstrates that the use of nonsense suppression could be a valuable therapeutic approach for blinding diseases caused by nonsense mutations.

INTRODUCTION

The extensive genetic and allelic heterogeneity observed within inherited eye diseases is a major barrier to the development of therapeutics. Leber congenital amaurosis (LCA) is a typical example, in which more than 400 mutations have been identified in 19 different genes.[1] Even in diseases associated with a single gene, significant variation is seen. For example, more than 600 mutations in a single gene (*PAX6*) cause aniridia.[2] Developing preventative treatments for these congenital diseases would also theoretically have to overcome the ethical and technical barriers associated with prenatal treatment. However, a meta-analysis of mutations that cause human disease has shown that approximately 12% of genetic diseases occur because of nonsense mutations.[3] Examining sequencing data for LCA and aniridia, in-frame nonsense mutations account for approximately 35%[1] and 50% of cases,[2] respectively. Therefore, a treatment targeted at nonsense suppression could have the potential to treat many patients with inherited eye disease.

Nonsense mutations coding for a premature termination codon (PTC) in an mRNA template lead to either the production of a truncated polypeptide or, more frequently, the mRNA is destabilized by a surveillance mechanism known as nonsense-mediated mRNA decay,[4] so that little or no toxic protein is produced. PTCs can be overridden by alterations in the fidelity or efficiency of the termination process, thereby functionally suppressing the nonsense mutation. This nonsense suppression occurs during mRNA translation, in which a near-cognate aminoacyl tRNA is inserted into the polypeptide, replacing the stop codon. As long as the premature stop codon is not in a critical position for protein activity, then a functional protein could be produced.[5] This type of ribosomal misreading was recognized as an off-target effect of aminoglycoside antibiotics several decades ago.[6] Suppression of nonsense mutations has since been demonstrated in mammalian and patient-derived cell lines[5,7] and in a variety of pre-clinical animal models.[8,9] In previous work, we have also demonstrated this phenomenon in a number of models of inherited eye disease.[10,11] However, aminoglycosides are too toxic to be considered for long-term use in the clinical setting;[12] therefore, screens of small-molecule chemical libraries have identified compounds with nonsense suppression activity, including Ataluren,[12,13] RTC13,[14] and other chemical analogs.[15] Some of these compounds have already been tested in pre-clinical models[13,16] and in clinical trials.[17–19]

Aniridia is characterized by partial or complete absence of iris tissue at birth, progressive corneal opacity, cataract, glaucoma, foveal hypoplasia, and optic nerve defects and can be associated with Wilms' tumor and abnormalities of the brain, pancreas, and olfactory system.[20]

Received 4 November 2016; accepted 3 May 2017;
http://dx.doi.org/10.1016/j.omtn.2017.05.002.

Correspondence: Cheryl Y. Gregory-Evans, Department of Ophthalmology and Visual Sciences, University of British Columbia, 2550 Willow Street, Vancouver, BC V5Z 3N9, Canada.
E-mail: cge30@mail.ubc.ca

On the basis of our previous studies in nonsense suppression in the eye,[10,11] we most recently showed that nonsense suppression can also reverse the congenital ocular anomalies seen in a mouse model of aniridia.[21] Because each of the eye defects in aniridia occur at different times during disease pathogenesis and the underlying disease mechanism is caused by PAX6 haploinsufficiency,[22] we hypothesized that the tissues affected are sensitive to differing dosages of Pax6 at different times. In this study, we evaluated the efficacy of postnatal nonsense suppression therapy in the *Pax6*$^{Sey/+}$ mouse model of aniridia using different topical treatment paradigms and correlated this with histological and functional testing in vivo to study effects in the developing retina, cornea, and lens. The results provide the first in vivo evidence that Pax6 dosage may be critical for lens capsule development and integrity.

RESULTS

Efficacy of Nonsense Suppression Therapy on *Pax6*$^{Sey/+}$ Ocular Histopathology

Three different concentrations of Ataluren (0.25%, 0.5%, and 1.0%), in an eye drop formulation that we previously developed called "START" therapy,[21] was administered twice daily to both eyes of the semi-dominant *Pax6*$^{Sey/+}$ mouse carrying a nonsense mutation (G194X). Treatment began when the eyes opened at P14 and continued to P60. At P14, the *Pax6*$^{Sey/+}$ mouse eye was already malformed compared to wild-type (WT) (Figures 1A and 1C). The histological benefit we observed from topical START therapy treatment was dose dependent, but at all concentrations, we saw qualitative improvement in ocular pathology. In comparison to vehicle-treated WT eyes at P60 (Figure 1B), the vehicle-treated *Pax6*$^{Sey/+}$ had very abnormal pathology, with notable infolding of the retina and a small lens (Figure 1D). When eyes were treated with 0.25% START therapy, there appeared to be some rescue of the eye phenotype, but the lens was still smaller than normal and malformed, with retrolenticular pigmentary deposits on the lens, and adhesion of the iris to the posterior surface of the cornea was noted (Figure 1E). Dosing with 0.5% START therapy resulted in abnormal corneal and anterior lens structures, most likely resulting from failure of the lens stalk to separate from the surface ectoderm correctly during lens morphogenesis (Figure 1F). Furthermore, the posterior aspect of the lens was abnormal. The 1% START therapy dose resulted in an eye with a normal appearance of the retina, lens, iris, and cornea at P60 (Figure 1G). Dosing every third day with 1% START therapy resulted in corneal and lens defects similar to those observed with the 0.5% dose (Figure 1H). These data demonstrated that the 1% START dose formulation was the most efficacious in reversing the ocular pathology in the eye. To further establish the temporal effect of the 1% dose of START treatment on *Pax6*$^{Sey+}$ mouse eyes compared to WT eyes, histology was examined at the intermediate time points of P21, P30, and P45. At P21, after just 7 days of treatment, the retina and lens defects eye already appeared to look more normal (Figures 1I and 1M). However, the corneal stroma appeared to be thicker than the comparative vehicle-treated WT eye. By P30, the corneal stroma had become thinner, similar to WT eyes (Figure 1N). When 1% START therapy was used to treat *Pax6*$^{Sey\text{-}1Neu/+}$ mice that had a splice-site mutation in *Pax6*,[23] we saw no benefit (Figures 1L and 1P), confirming that START therapy was specific for nonsense mutations. Finally, when treatment was started at P14 and stopped at P45 and then the eyes were examined at P60, we did not see any reversal back to the original pathology, indicating that the changes to ocular structure were stable (Figure S1S).

To further investigate the efficacy of the treatment, we evaluated the anterior segment of the eye, the lens, and the retina at higher resolution. The lens was clearly malformed and attached to pigmented tissue with 0.25% START treatment (Figure 2A). Using either 0.5% START (Figure 2B) or 1% START every 3 days (Figure 2C), we observed remnants of the lenticular stalk in the lens and corneal stroma. We also identified breaks in the lens capsule with what appeared to be lenticular material in the vitreous cavity when using the 0.5% START dose (Figure 2D). Although the infolding defect of the retina was rescued at the lower doses, the outer nuclear layer (ONL) of the retina was about 30% thinner than that of WT (7 to 8 rows of nuclei versus 10 to 11 rows, respectively), and the inner nuclear layer (INL) was about 50% thinner than that of WT (Figures 2E–2H). Only with the 1% START dose did we observe almost full rescue of the retinal architecture (Figure 2I). We quantified the ratio of inner and outer nuclei cell counts in WT mouse eyes compared to the different treatment doses (Figure 2J), confirming that the 1.0% dose was the most efficacious.

We then sought to determine for how long after the eyes had opened that START therapy would be effective in reversing the pathological defects. For these studies, histological analysis was compared when treatment began at P21 (Figures 3A–3E) and P28 (Figures 3F–3J) using the 1% Ataluren dose in START therapy eye drops that was continued for 46 days to P67 or P74, respectively. Prior to the commencement of therapy at P21, untreated eyes were severely malformed compared to WT (Figures 3A and 3B), and vehicle treatment had no effect on the ocular pathology (Figure 3C). However, treatment with 1% START therapy beginning at P21 reversed the malformation defects of the lens and iris and partially rescued the retinal infolding (Figure 3D). In comparison, when treatment began at P28, the lens was abnormally large, almost filling the entire globe (Figures 3I–3K), there were breaks in the lens capsule, and lenticular material appeared to have been extruded into the vitreous cavity, similar to that seen when eyes were treated with a low dose (0.5% START) (Figure 1F). Despite the large lens, the eye was grossly less malformed compared to the vehicle-treated or untreated eyes (Figures 3G and 3H).

To further define the nature of the retrolenticular material in the lower doses of START therapy or when treatment started at a later developmental time point, we used a series of differential immunohistochemical markers. In untreated *Pax6*$^{Sey/+}$ eyes at P14 and P60 (Figures 1C and 1D), a pigmented mass posterior to the lens and extending to the retina was suggestive of failed regression of the primary vitreous and hyaloid vasculature, a critical event in eye

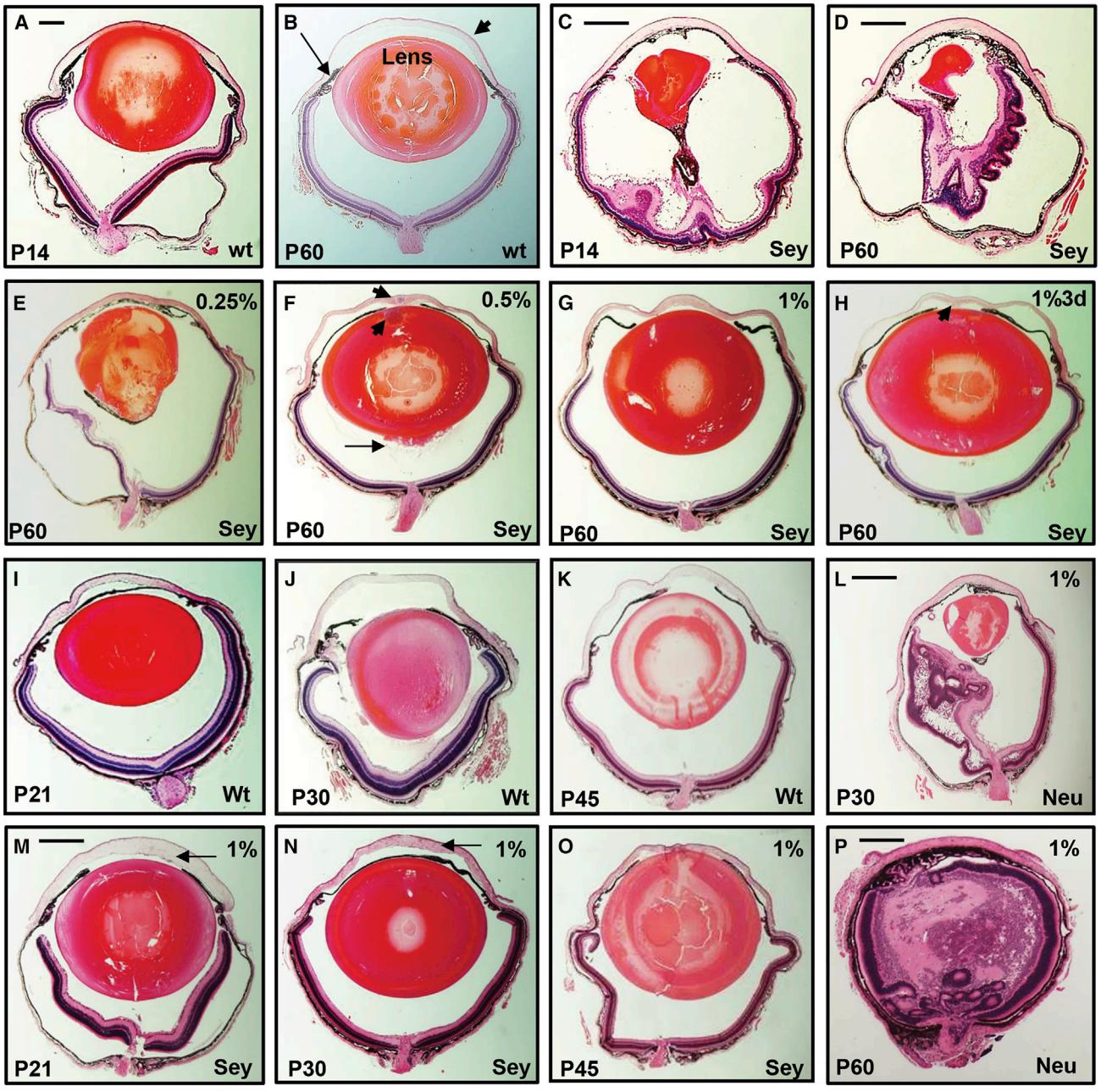

Figure 1. Efficacy of START Therapy on Ocular Histopathology

(A) Untreated WT *Pax6*$^{+/+}$ (wt) eye at start of treatment (P14). (B) Vehicle-treated *Pax6*$^{+/+}$ eye at end of treatment period (P60). Arrow, normal iris; arrowhead, normal cornea. (C) Untreated *Pax6*$^{Sey/+}$ nonsense mutant (Sey) eye at start of treatment (P14). (D) Vehicle-treated *Pax6*$^{Sey/+}$ eye at end of treatment (P60). (E) *Pax6*$^{Sey/+}$ eye, 0.25% Ataluren at P60. (F) *Pax6*$^{Sey/+}$ eye, 0.5% Ataluren at P60. Arrow, posterior lens defect; arrowheads, lens stalk remnant in cornea and lens. (G) *Pax6*$^{Sey/+}$ eye, 1% Ataluren at P60. (H) *Pax6*$^{Sey/+}$ eye, 1% Ataluren every 3 days (1%3d) at P60. Arrowhead, corneal/lens defect. (I) Vehicle-treated *Pax6*$^{+/+}$ eye at P21. (J) Vehicle-treated *Pax6*$^{+/+}$ eye at P30. (K) Vehicle-treated *Pax6*$^{+/+}$ eye at P45. (L) *Pax6*$^{Neu/+}$ mutant eye with splice-site mutation, 1.0% Ataluren at P30. (M) *Pax6*$^{Sey/+}$ eye, 1% Ataluren at P21. Arrow, thick corneal stroma. (N) *Pax6*$^{Sey/+}$ eye, 1% Ataluren at P30. Arrow, thin corneal stroma. (O) *Pax6*$^{Sey/+}$ eye, 1% Ataluren at P45. (P) *Pax6*$^{Neu/+}$ mutant eye with splice-site mutation, 1.0% Ataluren at P60. Scale bars, 500 μm (A) and 500 μm denoted by a longer bar (C, D, L, M, and P; the mutant eye is smaller than normal).

development.[23] To determine if the retrolenticular mass of treated eyes had remnants of hyaloid vasculature from the retina, sections of the eye were incubated with NG2 chondroitin sulfate proteoglycan, which labels pericytes that line the outer surface of endothelial cells of blood vessels. NG2 does not label the WT lens (Figure 4G), but does label the retinal vessels, as would be expected (Figure 4H).

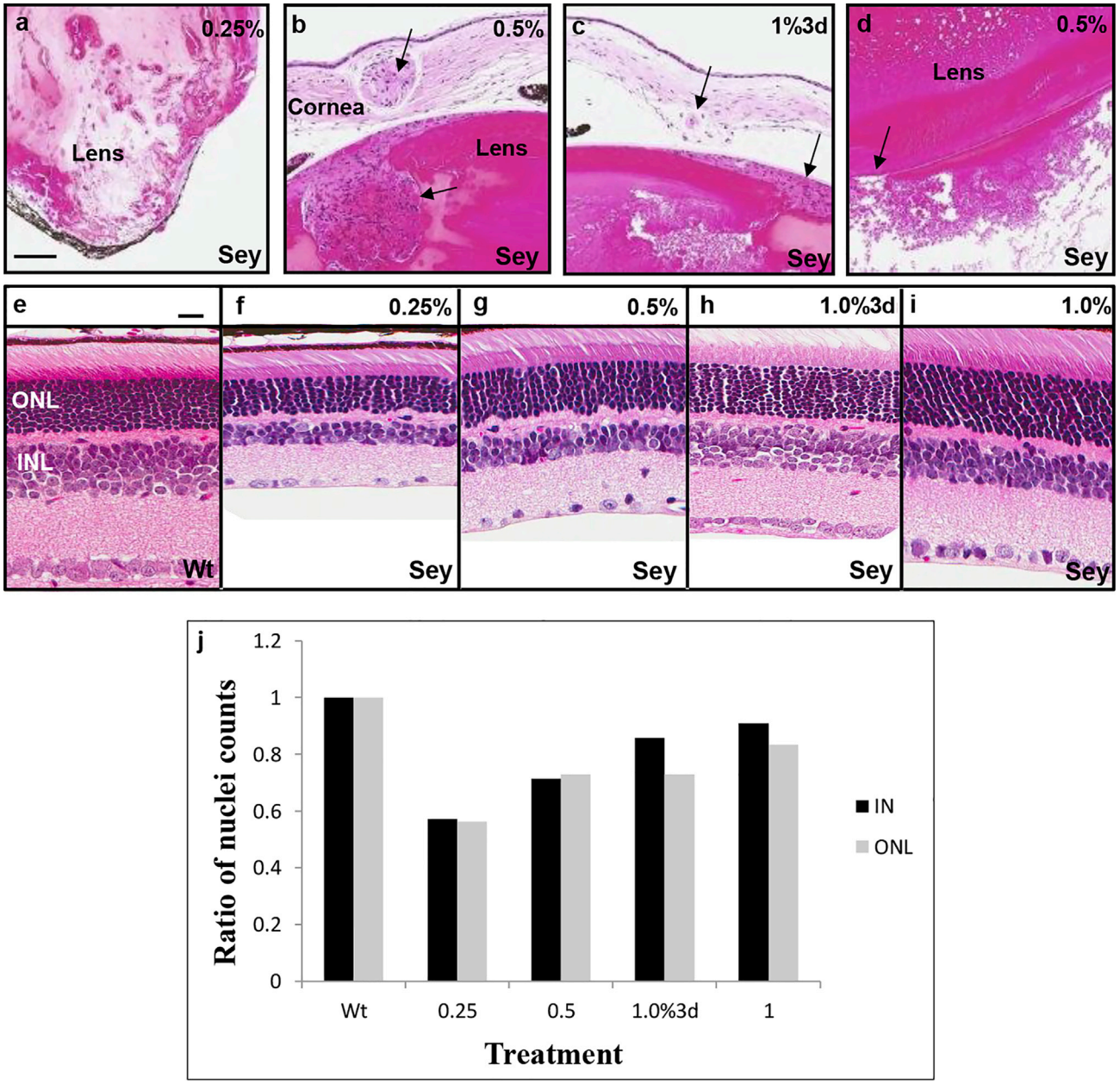

Figure 2. Histology of Abnormal Ocular Structures with Nonsense Suppression Treatment at P60

Representative H&E staining of paraffin-embedded sagittal sections of WT and *Pax6*$^{Sey/+}$ (Sey) eyes. (A) Posterior lens with pigmentary deposits, 0.25% START. (B) Anterior lens and cornea, 0.5% START. Arrows, lens stalk remnant. (C) Lens and cornea, 1% START every 3 days. Arrows, lens stalk remnant. (D) Posterior lens, 0.5% START. Arrow denotes break in lens capsule. Lenticular material is seen in the space outside of the lens. Scale bars, 100 μm (A–D). (E) WT retinal section in the sagittal plane. (F) Retina, 0.25% START. (G) Retina, 0.5% START. (H) Retina, 1.0% START every 3 days. (I) Retina, 1.0% START. Scale bars, 25 μm (E–I). (J) The ratio of inner (IN) and outer (ONL) layer nuclei in WT eyes compared to the different treatments (0.25%, 0.5%, and 1% every 3 days and 1.0% alone).

We observed that NG2 did not label the retrolenticular mass of treated eyes (Figures 4I–4L), indicating that vascular structures were absent. To determine if the retrolenticular mass contained proliferating cells, the ocular sections were labeled with Ki-67, a marker expressed in active cycling cells. Using 0.5% START therapy or using 1% beginning at P28, Ki-67-positive cells were observed in the retrolental mass (Figures 4O–4R), suggesting proliferation was occurring. The tissue nearest the lens capsule break was of lens origin because it was strongly labeled with αB-crystallin (Figures 4S–4X).

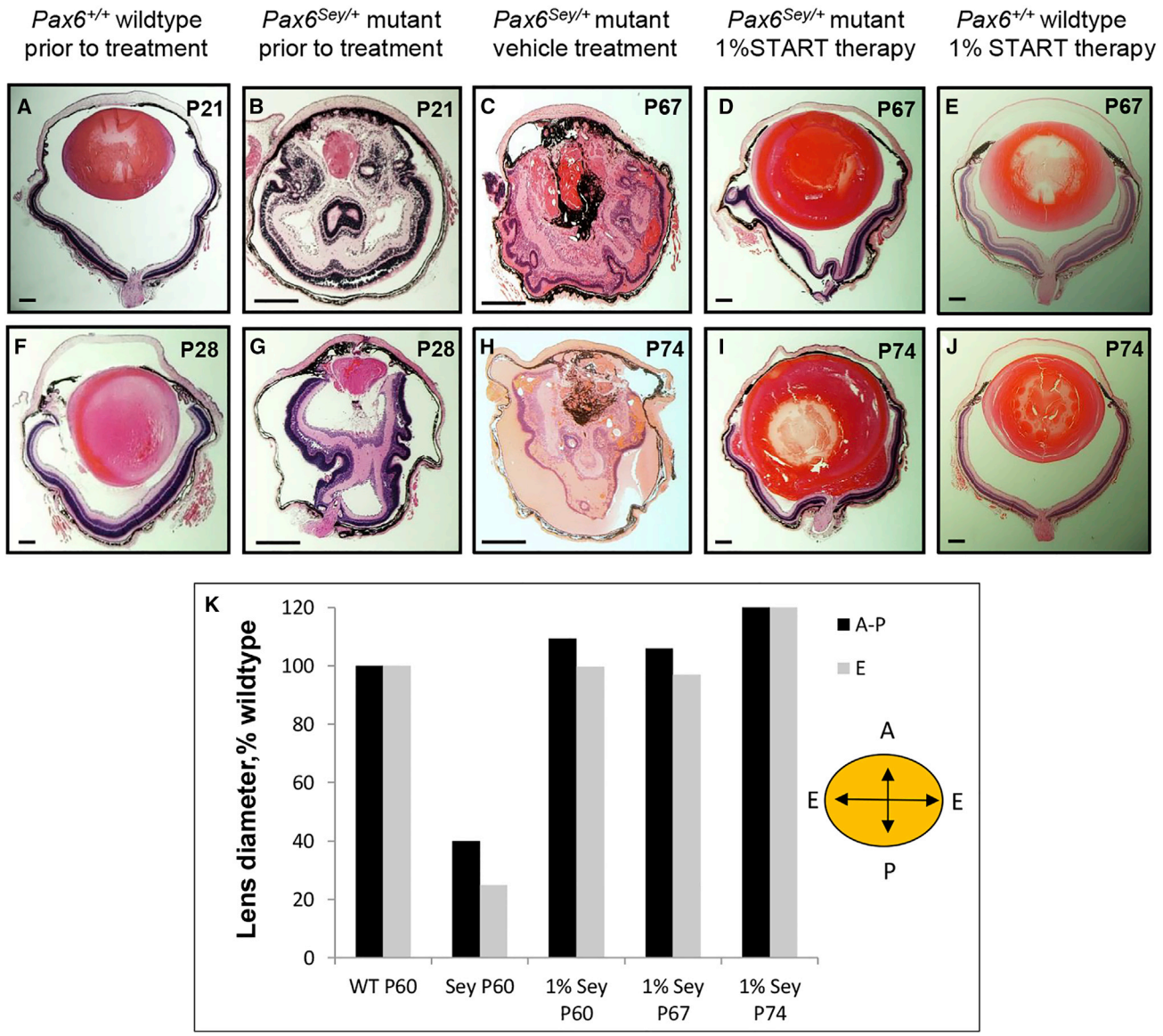

Figure 3. Comparison of Ocular Histology When START Therapy Was Initiated at Different Times

(A–E) Treatment began at P21 and ended at P67. (F–J) Treatment began at P28 and ended at P74. All treatments were 46 days long, and the START therapy contained 1% Ataluren. All sections are in the sagittal plane. Scale bars, 500 μm in all images. (K) The size of the lens relative to the WT size in the anterior-posterior axis (A-P) or equatorial axis (E), with the different treatments measured at P60, P67, or P74.

Nonsense Suppression Increases Pax6 and Mmp9 in the Cornea of *Pax6*$^{Sey/+}$ Mice

An established downstream target of the Pax6 transcription factor in the cornea is the *Mmp9* gene, which is required for the maintenance and repair of the corneal epithelium throughout life.[24] Therefore, we measured the amount of Pax6 and Mmp9 proteins in corneal epithelial extracts from *Pax6*$^{Sey/+}$ mice with the different START dosing regimens. There was a statistically significant increase in Pax6 levels compared to untreated controls ($F(9,40) = 101.458$, $p = 0.001$) with all treatments except when using the 0.25% START dose and the 1% dose every 3 days (Figure 5A). Similarly, a statistically significant increase in Mmp9 levels was observed ($F(9,40) = 117.013$, $p = 0.001$) with all treatments except when using the 0.25% START dose (Figure 5A). Immunoprecipitation followed by western blotting revealed a similar increase in protein expression with the different treatment doses (Figure 5B).

Functional Effects of Different Dosing Regimens in *Pax6*$^{Sey/+}$ Mice

To determine how the different START therapy regimens affected functional benefit, we first measured electroretinographic (ERG)

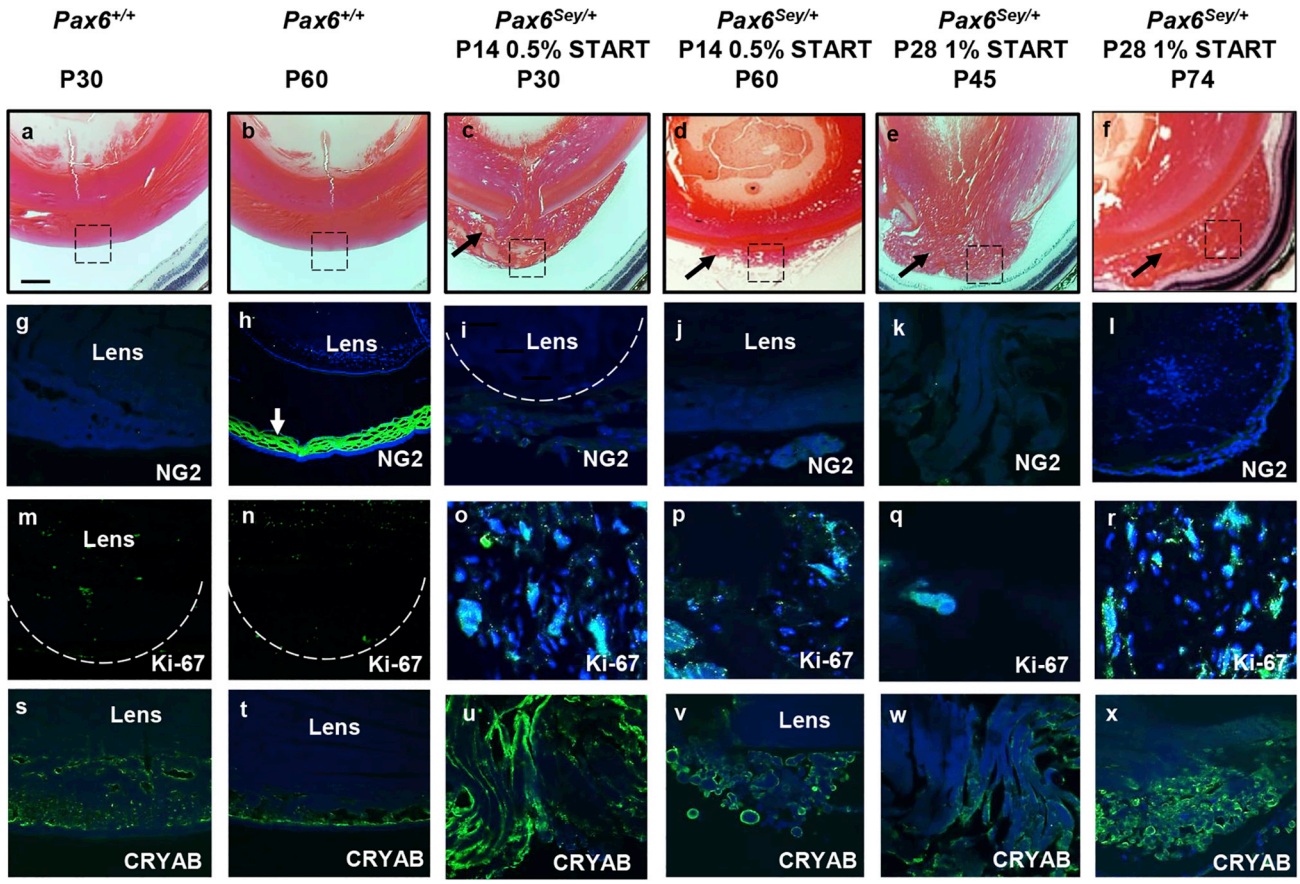

Figure 4. Immunocytochemical Analysis of the Retro-lenticular Tissue

(A–F) H&E stain showing lens defect in *Pax6*$^{Sey/+}$ eyes (black arrows) treated with either 0.5% Ataluren in START formulation beginning at P14 or 1% Ataluren in START formulation beginning at P28 compared to WT (*Pax6*$^{+/+}$). Scale bar, 500 μm. (G–L) Localization of vascular pericyte marker NG2 (green) in the retina (white arrow), but not in the lens or extra-lenticular material. Dotted line in (l) identifies the edge of the lens. (M–R) Ki-67 staining (green) present in the retrolental mass. (S–X) Localization of αB-crystallin (CRYAB) protein (green). All sections are in the sagittal plane.

responses of the retina to flashes of light. We examined scotopic, photopic, and oscillatory potentials and 12-Hz flicker responses. Mice receiving only vehicle treatment had unrecordable ERG traces in all tested parameters (Figure 6, trace 2). All START treatment regimens resulted in recordable ERG responses to varying degrees compared to untreated controls (Figure 6, traces 3–8). The three different doses of Ataluren resulted in a statistically significantly increase ($F(7,24)$ = 73.72, p = 0.001) in the scotopic maximal b-wave amplitudes compared to vehicle-treated mouse eyes (Figure 7). Critically though, only the 1.0% Ataluren dose gave ERG b-wave amplitudes that were not significantly different to a WT eye (p = 0.37). When the treatment started at either P21 or P28, the b-wave amplitudes were 81% and 48% of WT amplitudes, respectively. When START therapy was only administered every third day, significant functional benefit was still observed (46% of WT, $p < 0.01$). These smaller ERG responses correlated with the partial histological rescue in the retina.

To determine if the retinal responses to light led to a change in behavior, we carried out optokinetic tracking (OKT) analysis, which is a response mediated via the accessory optic system of the brain. This analysis tests the ability of an animal to track a moving stimulus and is an approximation of visual acuity.[25] Under standard OKT test conditions, untreated *Pax6*$^{Sey/+}$ mice demonstrated very limited tracking capability compared to WT controls (spatial frequency thresholds of 0.04 cyc/deg versus 0.42 cyc/deg, respectively). In contrast, *Pax6*$^{Sey/+}$ mice treated with increasing doses of Ataluren resulted in a statistically significant increase ($F(7,40) = 100.84$.p = 0.001) in tracking ability (Figure 7). Starting the treatment at either P21 or P28 resulted in an OKT tracking response that was significantly better (35% and 55% of WT, respectively; $p < 0.01$) than that of untreated mice (9% of WT), but did not improve the spatial frequency threshold by as much as when treatment started at P14 (90% of WT levels). The OKT tracking data plotted on the same graph as the ERG b-wave amplitudes showed a similar response pattern of dosing regimen for both functional testing paradigms (Figure 7).

DISCUSSION

In this study, we demonstrated that topical delivery of START therapy is an Ataluren dose-dependent response, with 1.0% Ataluren

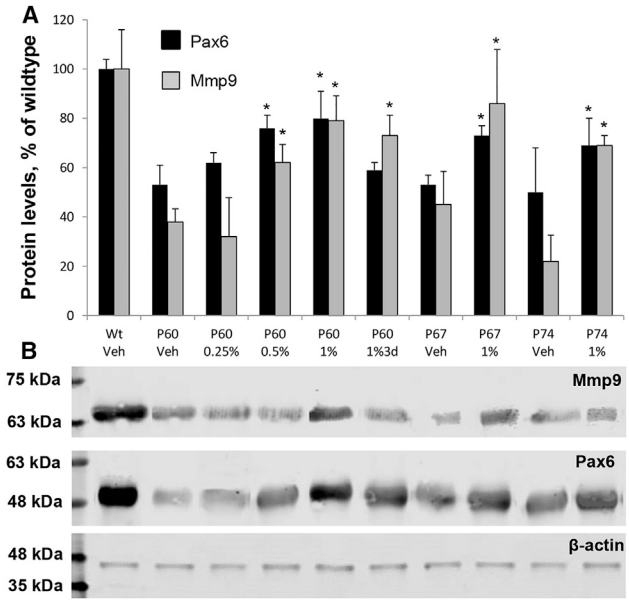

Figure 5. Expression of PAX6 and MMP9 Proteins in the Corneal Epithelium
(A) PAX6 protein (black bars) and MMP9 protein (gray bars) levels in *Pax6*$^{Sey+/-}$ corneal epithelium relative to Wt controls (set at 100%) using different doses of Ataluren in START eye drops. Veh, vehicle only. Treatment started at P14, P21, or P28 and continued for 46 days until P60, P67, or P74, respectively. All treated mice received START eye drops twice daily, except one group, which received drops every 3 days (1%3d). Data plotted as mean ± SEM (n = 5). *$p < 0.01$ when compared to vehicle-treated controls. (B) Directly below the graph is an immunoprecipitation experiment with the lane order as in the histogram above for PAX6, MMP9, and β-actin loading control. The molecular weight marker used was BLUelf pre-stained protein ladder (GeneDirex).

giving the best efficacy, as measured by histopathology, electroretinography, and behavioral testing. These data suggest that the postnatal mouse eye is remarkably sensitive to Pax6 dosage and is able to remodel under nonsense suppression therapy during a specific time window. We will not know how the timing of this remodeling would translate directly to the human eye until it is clinically tested. Nevertheless, the mouse START therapy data suggest that remodeling of abnormal tissue for ocular malformations associated with aniridia should start in the early postnatal years. It should be noted that the eye continues to develop in humans after birth. In particular, the fovea is not fully formed until about 4 to 5 years of age,[26,27] and foveal hypoplasia (an underdeveloped fovea) is present in up to 50%–70% of aniridia cases. Therefore, it is possible that START therapy early in life may be able to stimulate foveal development. Furthermore, if taken continuously throughout life, it may prevent the later onset of corneal keratopathy and may help in the management of refractory glaucoma.

We found that using 0.5% Ataluren or starting the treatment at P28 resulted in abnormalities to the posterior lens, suggesting that insufficient Pax6 dosage or expression of Pax6 at the incorrect time was deleterious. Through the ruptured lens capsule, lens fiber cells were extruded into the vitreous cavity, an uncommon but striking phenomenon observed in several other mouse mutants (*Ilk*, *Abi2*, *Bcar3*).[28–30] Although these examples are gene specific and show high levels of penetrance, the rupture of the lens capsule could be a secondary event due to failure of hyaloid vasculature regression.[23] Alternatively, because the posterior capsule is produced by the newly differentiated lens fiber cells,[31] then a primary lens fiber defect could precipitate capsule rupture, as seen in the SPARC-deficient mice.[32] The lens capsule is continually remodeled throughout life; thus, our data suggest that Pax6 may have a direct role in lens capsule development or maintenance. Further independent studies would be required to demonstrate the exact role of Pax6 in lens capsule homeostasis. However, given that Pax6 is known to regulate the major constituents of the extracellular matrix proteins in the capsule (fibronectin 1, versican, and collagen)[33,34] and the clinical evidence in aniridic patients who are prone to lens capsule rupture during cataract surgery,[35] this suggests that Pax6 is critical to lens capsule fidelity.

The unusually large lens present in *Pax6*$^{Sey/+}$ mice (C57BL/6 background) treated with START therapy beginning at P28 is intriguing because this phenotype has not been observed in other *Pax6* mouse models.[36,37] In normal C57BL/6 mice, there is a rapid postnatal increase in lens diameter from P22 to P47 (~1.47 mm to 1.7 mm) and, thereafter, lens growth slows, reaching steady state (~1.8 mm) by P81.[38] Therefore, perhaps manipulating Pax6 dosage at P28, leading to lens capsule rupture, might allow unconstrained expansion of the lens during its normal growth period. Little is known about the genes that modulate the rate and duration of normal postnatal lens growth. However, in C57BL/6 mice, the *Eye1* locus on chromosome 5 was identified as a quantitative trait locus (QTL) associated with increased lens weight at P75.[39] The *Eye1* QTL was identified by the microsatellite marker *D5mit346* located in the *Cdk14* gene on chromosome 5q. Tight linkage in the genomic region from *Fzd1* to *Hgf* (containing *D5mit346*) comprises 17 annotated genes (Table S1) according to the Genome Reference Consortium assembly m38 (January 2012). Five of these genes (*Fzd1*, *Adam22*, *Sema3d*, *Sema3a*, and *Hgf*) are expressed in the developing lens,[40–44] but expression in the adult lens has only been reported for *Hgf*.[45] Targeted deletion of each of the five genes in mice has been reported; however, the lens was not examined in any of these studies; thus, their role in lens growth cannot be inferred. Interestingly, Hgf has been shown to stimulate lens epithelial cell proliferation and overexpression causes opacification of the posterior lens capsule.[46] This suggests that Hgf could be the major contributing factor at the *Eye1* QTL; however, whether Pax6 has a direct or indirect role in *Hgf* expression in the lens remains to be determined.

Another consistent defect we observed were remnants of an ectodermal plug in the cornea and anterior lens when using low doses of Ataluren (0.5% or 1% every 3 days), which is reminiscent of previous phenotypic data reported in the *Pax6* heterozygous eye.[47] This feature has been shown to be due to an autonomous deficiency of Pax6 in the lens epithelium, but not due to Pax6 loss in the corneal tissue.[47,48] Some patients with *PAX6* mutations similarly show incomplete separation of the lens from the cornea (Peter's anomaly),

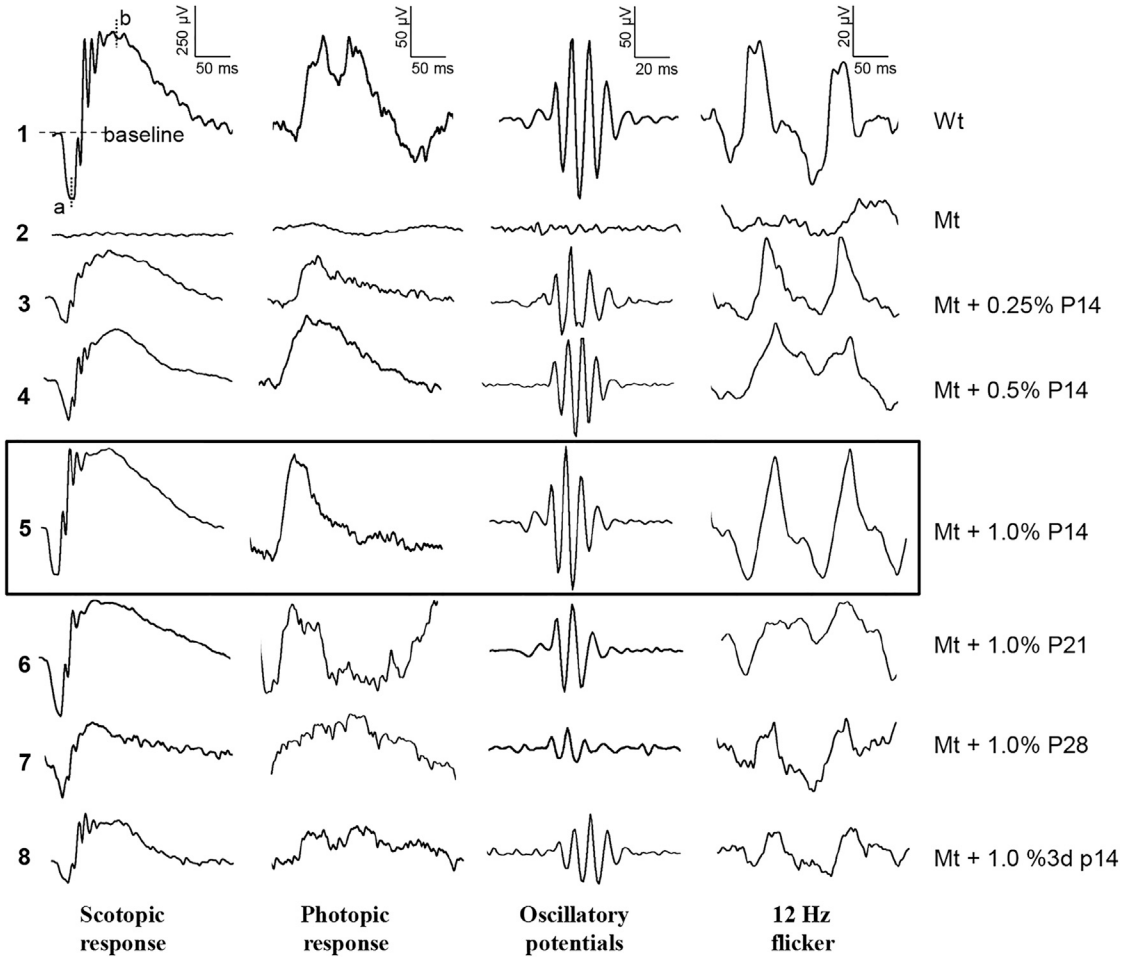

Figure 6. Representative ERG Recordings for Different START Therapy Regimens

Trace 1, vehicle-treated WT *Pax6*$^{+/+}$ responses. a, a-wave maximum from baseline (µV); b, b-wave maximum from baseline (µV). Trace 2, *Pax6*$^{Sey+/-}$ untreated responses. Trace 3, *Pax6*$^{Sey+/-}$ with 0.25% Ataluren from P14. Trace 4, *Pax6*$^{Sey+/-}$ with 0.5% Ataluren from P14. Trace 5, *Pax6*$^{Sey+/-}$ with 1% Ataluren from P14. Trace 6, *Pax6*$^{Sey+/-}$ with 1% Ataluren from P21. Trace 7, *Pax6*$^{Sey+/-}$ with 1% Ataluren from P28. Trace 8, *Pax6*$^{Sey+/-}$ with 1% Ataluren every third day. Trace 5 is boxed because it gave the best response compared to WT.

which normally occurs between the fourth and seventh week of embryonic development. Our data in mice suggest that insufficient levels of nonsense suppression in the lens compromise its ability to induce the necessary interactions that organize anterior segment development. Delivery of the nonsense suppression drug to the lens at an earlier time point than P14 would be an important area to target in the future.

The ability of Ataluren to suppress the nonsense mutation depends on the specific termination codon, the nucleotide immediately downstream of the nonsense codon, and the location in the mRNA template.[12,13] It should be noted that the normal termination codon in the mRNA template is not suppressed by Ataluren.[13,49] There is a higher readthrough capacity for UGA codons compared to UAA codons. Thus, for any given patient mutation, it would be possible to predict how well nonsense suppression might work. However, another consideration is what amino acid replaces the premature stop codon and whether it affects a critical functional protein domain? A recent report showed that the most frequent amino acid replacements at a UAA codon with Ataluren treatment was Gln (52%), Lys (46%), or Tyr (2%), whereas as at UAA codons, the frequency of insertions was Gln (88%), Tyr (95%), and Lys (35%).[50] At UGA codons, the insertions were Trp (87%), Cys (9%), or Arg (5%). In this study, the *Pax6*$^{Sey/+}$ mouse premature termination codon is UGA, so the normal Gly194 would most likely be replaced by Trp amino acid. The Gly194 residue is located in the flexible linker region of the Pax6 protein between the functionally important paired and homeodomains. Thus, presumably, the inserted amino acid can be tolerated in the linker region. A further consideration regarding nonsense suppression efficiency is the effect of nonsense-mediated mRNA decay (NMD).[51] Because the efficiency of PTC readthrough is often low,[12] improving the nonsense suppression approach could

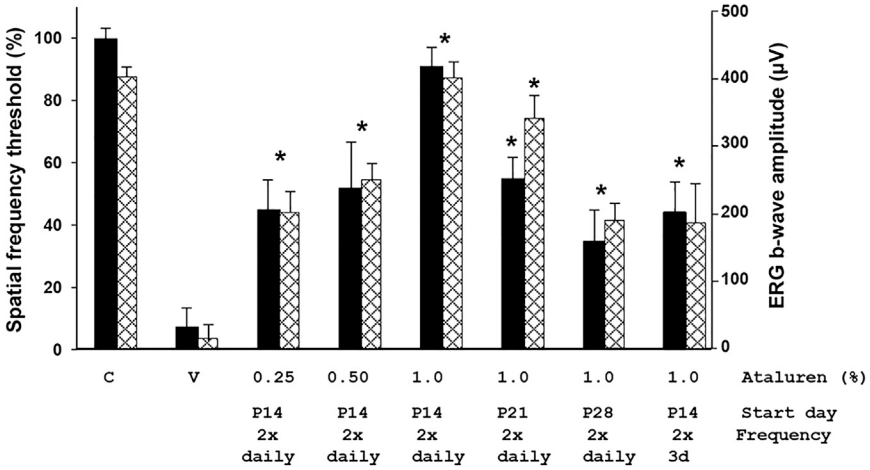

Figure 7. Comparison of OKT and ERG Data with Different START Therapy Treatment Regimens

Spatial frequency threshold (filled bars) and b-wave amplitudes (hatched bars) for control *Pax6*$^{+/+}$ mice (C) and vehicle-treated *Pax6*$^{Sey/+}$ mice (V) compared to data from treated *Pax6*$^{Sey/+}$ mice using different doses of Ataluren in the START eye drop formulation. Treatment started at P14, P21, or P28 and continued for 46 days to P60, P67, or P74, respectively. All treated mice received START eye drops twice daily, except one group, which received drops every 3 days (3d). Data plotted as mean ± SEM, n = 6. *$p < 0.01$ when comparing to vehicle-treated controls.

involve using a combination of drugs, which lead to suppression of ribosomal misreading and inhibition of NMD. By inhibiting NMD, the mutant mRNA transcript would be available for longer, allowing the nonsense suppression drugs to make more protein.

Although nonsense suppression is still in its infancy from a clinical perspective, it represents an exciting therapeutic avenue for a subgroup of currently untreatable genetic eye diseases. In terms of assessing nonsense suppression in clinical trials, defining the therapeutic end-point that correlates with therapeutic efficacy may be challenging. This is especially pertinent if there is a wide phenotypic variability in patients because it might be difficult to detect the clinical benefit if there is less than a 20% increase in protein function. Furthermore, because different tissues respond to different doses of nonsense suppression drug, then more than one route of administration and the timing of different doses may be needed. Moreover, identifying patients with nonsense mutations will require significant resources to be invested. Nevertheless, as a pharmacological approach to overcome genetic eye diseases, nonsense suppression has the potential to become routine practice in the future for many patients carrying nonsense mutations.

MATERIALS AND METHODS

Animals

All studies were carried out with the approval of the Animal Care Committee at the University of British Columbia, and in accordance with the Association for Research in Vision and Ophthalmology Statement for the Use of Animals in Ophthalmic and Vision Research. Mice were housed under cyclic light (14 hr on: 10 hr off) and had access to food and water ad libitum. Mice were maintained on the C57BL/6 background strain, and *Pax6* $^{Sey/+}$ mutant offspring were identified by genotyping. Genomic tail DNA was prepared using a REDExtract-N-Amp Tissue PCR kit (Sigma-Aldrich). Using GoTaq Mastermix (Promega), 250 nM of each PCR primer, and 4 μL of extracted DNA tissue mix, PCR products were amplified using an initial cycle of 95°C for 3 min, 55°C for 1 min, and 72°C for 1 min, followed by 35 cycles of 1 min at 95°C, 40 s at 55°C, and 40 s at 72°C. Primers were as follows: forward SP1 (annealing to the *Sey* allele): 5′-GAGAACACCAACTCCATCA GTTCTAAGT-3′; forward SP2 (annealing to the WT allele): 5′-AGCAACAGGAAGGAGGGGGAACGAAC ACCAACTCCATCAGTTCTTACG-3′; reverse MC130 primer for both PCR reactions: 5′-CTTTCTCCAGAGCCTCAATCTG-3′. PCR-amplified DNA was analyzed on a 3% TBE agarose gel. The WT allele produces a 148-bp SP2/MC130 band, and the *Pax6*^{sey} allele generates a 129-bp SP1/MC130 band, as previously described.[52]

Drug Administration

The topical eye drop START formulation (0.9% sodium chloride, 1% Tween 80, powdered Ataluren, and 1% carboxy methylcellulose) was prepared as previously described[21] and contained either 0.25%, 0.5%, or 1% Ataluren (Selleckchem). START eye drops were instilled into both eyes twice daily beginning at either P14, P21, or P28 and continuing until analysis at P60, P67, and P74, respectively. In an alternative paradigm, eyes received drops twice every third day from P14 to P60. Efficacy of the treatment was assessed by OKT and electroretinography, followed by histology and ELISA.

OKT

We assessed behavioral responses by measuring the spatial frequency threshold during OKT, as previously described,[25] using rodent-specific OptoMotry software (Cerebral Mechanics). Briefly, a virtual cylinder was created that comprised a vertical sine wave grating projected onto four computer monitors that surrounded a platform that the mice were placed upon. The cylinder was rotated at 12 deg/s, and the head tracking was monitored via a video camera. The highest spatial frequency capable of driving the head tracking response was adopted as the threshold (photopic intensity, 142 cd/m^2).

Electroretinography

Mice were dark adapted for 2 hr prior to testing and then anesthetized with a mixture of intraperitoneal ketamine (70 mg/kg, Vetalar, Bioniche Animal Health) and xylazine (4.5 mg/kg, Rompun, Bayer Healthcare). To dilate the pupil, 0.5% tropicamide (Bausch and Lomb) was administered topically. After a drop of Viscotears eye lubrication was applied to each eye, contact lens electrodes were

placed on the eyes. To test the responsiveness of the retina to light flashes, we used an Espion E2 system with a Colordome mini-Ganzfeld stimulator (Diagnosys), as previously described.[10] Dark-adapted responses were recorded at P60 by averaging 15 responses at a stimulus intensity of 3.16 cd s/m^2. Light-adapted cone responses were carried out in 30 cd/m^2 background light.

Histology and Immunocytochemistry

Mouse eyes were enucleated and then fixed in Karnovsky's fixative for 2 hr prior to embedding in paraffin wax. Sections were stained with H&E and photographed using an Aperio ScanScope digital scanning system (Leica Biosystems). The eyes for immunohistochemistry were fixed in 4% paraformaldehyde overnight and then infiltrated with 30% sucrose at 4°C before embedding in Polyfreeze medium (Polysciences). Immunolabeling was carried out using 6- to 10-μm-thick frozen sections. The following primary antibodies were used: NG2 monoclonal (1:200, Abcam, ab50009); Ki-67 polyclonal (1:500, Abcam, ab15580); and Alpha B Crystallin (CRYAB) monoclonal (1:200, Abcam, ab13496). Secondary antibodies used were Alexa Fluor 488 goat anti-rabbit immunoglobulin G (IgG) or Alexa Fluor 488 goat anti-mouse IgG (Life Technologies). Sections were incubated overnight at 4°C with primary antibody diluted in blocking buffer. After extensive washes in PBS-Tween-20, localization of antibody labeling was detected after a 1-hr incubation, with secondary antibodies diluted in PBS containing 2% normal goat serum. Nuclei were counterstained with DAPI, and then images were acquired using scanning laser microscopy.

Protein Analysis Methodologies

The second eye from each mouse was used for ELISA analysis or western blotting. Corneal epithelium was dissected from the ocular surface into 100 μL of 1X PBS. The eye was opened at the limbus, and the retina was removed and placed into 100 μL of PBS. Tissue samples were then homogenized, followed by two freeze-thaw cycles. Homogenates were centrifuged for 5 min at 5,000 × *g*. The amount of Pax6 and Mmp9 in the supernatant was compared to a standard curve using either a mouse PAX6 or MMP9 ELISA kit (MyBioSource) according to the manufacturer's instructions. For immunoprecipitation, the same amount of protein from homogenate supernatants was immunoprecipitated with antibodies to PAX6 and MMP9 using SureBeads Protein G Magnetic Beads (Bio-Rad) according to the manufacturer's instructions. A 10% w/v SDS-PAGE gel was used to separate proteins, which were then transferred to Immobilon-FL membrane (Millipore). Blocking of membranes was carried out in 5% non-fat dry milk powder in PBS/0.1% Tween-20 (PBST) for 1 hr at room temperature. Following three washes in PBST, the membranes were incubated with PAX6 polyclonal (1:300, Biolegend, 901301), MMP9 monoclonal (1:2,000, Abcam, ab76003), and β-actin monoclonal (1:3,000, Sigma, A5316) at 4°C overnight. The membranes were washed 3x for 20 min with PBST in the dark. Anti-rabbit IgG DyLight 800 (1:1,000, Rockland, 611-145-002) and anti-mouse IgG DyLight 680 (1:2,000, Rockland, 610-144-002) were used as the secondary antibodies. Visualization of protein was performed in the Odyssey LI-COR imaging system. The molecular weight marker used was BLUelf pre-stained protein ladder (GeneDirex).

Statistical Analysis

Analyses were performed with GraphPad Prism 5.0. For parameter comparisons between groups, an unpaired Student's t test was used. p values of less than 0.05 were considered significant. Results are reported as mean ± SEM. Multiple group comparison was performed by one-way ANOVA, followed by Tukey post hoc tests. Differences were considered significant at $p < 0.05$. Results are reported as mean ± SEM.

SUPPLEMENTAL INFORMATION

Supplemental Information includes one figure and can be found with this article online at http://dx.doi.org/10.1016/j.omtn.2017.05.002.

AUTHOR CONTRIBUTIONS

X.W. and C.Y.G-E. designed and performed the experiments. X.W., K.G-E., K.M.W., and C.Y.G-E. drafted the manuscript. O.S. and X.H. were responsible for sample collection and data analysis. All authors discussed, revised, and approved the manuscript.

CONFLICTS OF INTEREST

The authors have no conflicts of interest to declare.

ACKNOWLEDGMENTS

Funding for this work was provided by the Sharon Stewart Testamentary Fund. The mouse *Pax6*$^{Sey+/-}$ allele was provided by Dr. Veronica van Heyningen (MRC Human Genetics Unit), and the *Pax6*$^{Neu-1}$ allele was provided by Dr. Elizabeth Simpson (Centre for Molecular Medicine and Therapeutics, University of British Columbia).

REFERENCES

1. Wang, X., Wang, H., Sun, V., Tuan, H.F., Keser, V., Wang, K., Ren, H., Lopez, I., Zaneveld, J.E., Siddiqui, S., et al. (2013). Comprehensive molecular diagnosis of 179 Leber congenital amaurosis and juvenile retinitis pigmentosa patients by targeted next generation sequencing. J. Med. Genet. *50*, 674–688.

2. Tzoulaki, I., White, I.M., and Hanson, I.M. (2005). PAX6 mutations: genotype-phenotype correlations. BMC Genet. *6*, 27.

3. Mort, M., Ivanov, D., Cooper, D.N., and Chuzhanova, N.A. (2008). A meta-analysis of nonsense mutations causing human genetic disease. Hum. Mutat. *29*, 1037–1047.

4. Peltz, S.W., Brown, A.H., and Jacobson, A. (1993). mRNA destabilization triggered by premature translational termination depends on at least three cis-acting sequence elements and one trans-acting factor. Genes Dev. *7*, 1737–1754.

5. Keeling, K.M., Wang, D., Conard, S.E., and Bedwell, D.M. (2012). Suppression of premature termination codons as a therapeutic approach. Crit. Rev. Biochem. Mol. Biol. *47*, 444–463.

6. Burke, J.F., and Mogg, A.E. (1985). Suppression of a nonsense mutation in mammalian cells in vivo by the aminoglycoside antibiotics G-418 and paromomycin. Nucleic Acids Res. *13*, 6265–6272.

7. Bedwell, D.M., Kaenjak, A., Benos, D.J., Bebok, Z., Bubien, J.K., Hong, J., Tousson, A., Clancy, J.P., and Sorscher, E.J. (1997). Suppression of a CFTR premature stop mutation in a bronchial epithelial cell line. Nat. Med. *3*, 1280–1284.

8. Barton-Davis, E.R., Cordier, L., Shoturma, D.I., Leland, S.E., and Sweeney, H.L. (1999). Aminoglycoside antibiotics restore dystrophin function to skeletal muscles of *mdx* mice. J. Clin. Invest. *104*, 375–381.

9. Du, M., Jones, J.R., Lanier, J., Keeling, K.M., Lindsey, J.R., Tousson, A., Bebök, Z., Whitsett, J.A., Dey, C.R., Colledge, W.H., et al. (2002). Aminoglycoside suppression of a premature stop mutation in a Cftr-/- mouse carrying a human CFTR-G542X transgene. J. Mol. Med. (Berl.) *80*, 595–604.

10. Guerin, K., Gregory-Evans, C.Y., Hodges, M.D., Moosajee, M., Mackay, D.S., Gregory-Evans, K., and Flannery, J.G. (2008). Systemic aminoglycoside treatment in rodent models of retinitis pigmentosa. Exp. Eye Res. *87*, 197–207.

11. Moosajee, M., Gregory-Evans, K., Ellis, C.D., Seabra, M.C., and Gregory-Evans, C.Y. (2008). Translational bypass of nonsense mutations in zebrafish rep1, pax2.1 and lamb1 highlights a viable therapeutic option for untreatable genetic eye disease. Hum. Mol. Genet. *17*, 3987–4000.

12. Peltz, S.W., Morsy, M., Welch, E.M., and Jacobson, A. (2013). Ataluren as an agent for therapeutic nonsense suppression. Annu. Rev. Med. *64*, 407–425.

13. Welch, E.M., Barton, E.R., Zhuo, J., Tomizawa, Y., Friesen, W.J., Trifillis, P., Paushkin, S., Patel, M., Trotta, C.R., Hwang, S., et al. (2007). PTC124 targets genetic disorders caused by nonsense mutations. Nature *447*, 87–91.

14. Jung, M.E., Ku, J.M., Du, L., Hu, H., and Gatti, R.A. (2011). Synthesis and evaluation of compounds that induce readthrough of premature termination codons. Bioorg. Med. Chem. Lett. *21*, 5842–5848.

15. Du, L., Jung, M.E., Damoiseaux, R., Completo, G., Fike, F., Ku, J.M., Nahas, S., Piao, C., Hu, H., and Gatti, R.A. (2013). A new series of small molecular weight compounds induce read through of all three types of nonsense mutations in the ATM gene. Mol. Ther. *21*, 1653–1660.

16. Kayali, R., Ku, J.M., Khitrov, G., Jung, M.E., Prikhodko, O., and Bertoni, C. (2012). Read-through compound 13 restores dystrophin expression and improves muscle function in the mdx mouse model for Duchenne muscular dystrophy. Hum. Mol. Genet. *21*, 4007–4020.

17. Bushby, K., Finkel, R., Wong, B., Barohn, R., Campbell, C., Comi, G.P., Connolly, A.M., Day, J.W., Flanigan, K.M., Goemans, N., et al.; PTC124-GD-007-DMD STUDY GROUP (2014). Ataluren treatment of patients with nonsense mutation dystrophinopathy. Muscle Nerve *50*, 477–487.

18. Sermet-Gaudelus, I., Boeck, K.D., Casimir, G.J., Vermeulen, F., Leal, T., Mogenet, A., Roussel, D., Fritsch, J., Hanssens, L., Hirawat, S., et al. (2010). Ataluren (PTC124) induces cystic fibrosis transmembrane conductance regulator protein expression and activity in children with nonsense mutation cystic fibrosis. Am. J. Respir. Crit. Care Med. *182*, 1262–1272.

19. Hirawat, S., Welch, E.M., Elfring, G.L., Northcutt, V.J., Paushkin, S., Hwang, S., Leonard, E.M., Almstead, N.G., Ju, W., Peltz, S.W., et al. (2007). Safety, tolerability, and pharmacokinetics of PTC124, a nonaminoglycoside nonsense mutation suppressor, following single- and multiple-dose administration to healthy male and female adult volunteers. J. Clin. Pharmacol. *47*, 430–444.

20. Lee, H., Khan, R., and O'Keefe, M. (2008). Aniridia: current pathology and management. Acta Ophthalmol. *86*, 708–715.

21. Gregory-Evans, C.Y., Wang, X., Wasan, K.M., Zhao, J., Metcalfe, A.L., and Gregory-Evans, K. (2014). Postnatal manipulation of *Pax6* dosage reverses congenital tissue malformation defects. J. Clin. Invest. *124*, 111–116.

22. Dorà, N., Ou, J., Kucerova, R., Parisi, I., West, J.D., and Collinson, J.M. (2008). PAX6 dosage effects on corneal development, growth, and wound healing. Dev. Dyn. *237*, 1295–1306.

23. Saint-Geniez, M., and D'Amore, P.A. (2004). Development and pathology of the hyaloid, choroidal and retinal vasculature. Int. J. Dev. Biol. *48*, 1045–1058.

24. Sivak, J.M., West-Mays, J.A., Yee, A., Williams, T., and Fini, M.E. (2004). Transcription factors Pax6 and AP-2alpha interact to coordinate corneal epithelial repair by controlling expression of matrix metalloproteinase gelatinase B. Mol. Cell. Biol. *24*, 245–257.

25. Douglas, R.M., Alam, N.M., Silver, B.D., McGill, T.J., Tschetter, W.W., and Prusky, G.T. (2005). Independent visual threshold measurements in the two eyes of freely moving rats and mice using a virtual-reality optokinetic system. Vis. Neurosci. *22*, 677–684.

26. Hendrickson, A., Possin, D., Vajzovic, L., and Toth, C.A. (2012). Histologic development of the human fovea from midgestation to maturity. Am. J. Ophthalmol. *154*, 767–778.e2.

27. Gregory-Evans, C.Y., and Gregory-Evans, K. (2011). Foveal hypoplasia: the case for arrested development. Expert Rev. Ophthalmol. *6*, 565–574.

28. Teo, Z.L., McQueen-Miscamble, L., Turner, K., Martinez, G., Madakashira, B., Dedhar, S., Robinson, M.L., and de Iongh, R.U. (2014). Integrin linked kinase (ILK) is required for lens epithelial cell survival, proliferation and differentiation. Exp. Eye Res. *121*, 130–142.

29. Grove, M., Demyanenko, G., Echarri, A., Zipfel, P.A., Quiroz, M.E., Rodriguiz, R.M., Playford, M., Martensen, S.A., Robinson, M.R., Wetsel, W.C., et al. (2004). ABI2-deficient mice exhibit defective cell migration, aberrant dendritic spine morphogenesis, and deficits in learning and memory. Mol. Cell. Biol. *24*, 10905–10922.

30. Near, R.I., Smith, R.S., Toselli, P.A., Freddo, T.F., Bloom, A.B., Vanden Borre, P., Seldin, D.C., and Lerner, A. (2009). Loss of AND-34/BCAR3 expression in mice results in rupture of the adult lens. Mol. Vis. *15*, 685–699.

31. Johnson, M.C., and Beebe, D.C. (1984). Growth, synthesis and regional specialization of the embryonic chicken lens capsule. Exp. Eye Res. *38*, 579–592.

32. Yan, Q., Clark, J.I., Wight, T.N., and Sage, E.H. (2002). Alterations in the lens capsule contribute to cataractogenesis in SPARC-null mice. J. Cell Sci. *115*, 2747–2756.

33. Wolf, L.V., Yang, Y., Wang, J., Xie, Q., Braunger, B., Tamm, E.R., Zavadil, J., and Cvekl, A. (2009). Identification of pax6-dependent gene regulatory networks in the mouse lens. PLoS ONE *4*, e4159.

34. Huang, J., Rajagopal, R., Liu, Y., Dattilo, L.K., Shaham, O., Ashery-Padan, R., and Beebe, D.C. (2011). The mechanism of lens placode formation: a case of matrix-mediated morphogenesis. Dev. Biol. *355*, 32–42.

35. Neuhann, I.M., and Neuhann, T.F. (2010). Cataract surgery and aniridia. Curr. Opin. Ophthalmol. *21*, 60–64.

36. Duncan, M.K., Xie, L., David, L.L., Robinson, M.L., Taube, J.R., Cui, W., and Reneker, L.W. (2004). Ectopic Pax6 expression disturbs lens fiber cell differentiation. Invest. Ophthalmol. Vis. Sci. *45*, 3589–3598.

37. Favor, J., Gloeckner, C.J., Neuhäuser-Klaus, A., Pretsch, W., Sandulache, R., Saule, S., and Zaus, I. (2008). Relationship of Pax6 activity levels to the extent of eye development in the mouse, *Mus musculus*. Genetics *179*, 1345–1355.

38. Schedl, A., Ross, A., Lee, M., Engelkamp, D., Rashbass, P., van Heyningen, V., and Hastie, N.D. (1996). Influence of PAX6 gene dosage on development: overexpression causes severe eye abnormalities. Cell *86*, 71–82.

39. Zhou, X., Shen, M., Xie, J., Wang, J., Jiang, L., Pan, M., Qu, J., and Lu, F. (2008). The development of the refractive status and ocular growth in C57BL/6 mice. Invest. Ophthalmol. Vis. Sci. *49*, 5208–5214.

40. Zhou, G., and Williams, R.W. (1999). *Eye1* and *Eye2*: gene loci that modulate eye size, lens weight, and retinal area in the mouse. Invest. Ophthalmol. Vis. Sci. *40*, 817–825.

41. Stark, M.R., Biggs, J.J., Schoenwolf, G.C., and Rao, M.S. (2000). Characterization of avian frizzled genes in cranial placode development. Mech. Dev. *93*, 195–200.

42. Yan, X., Lin, J., Rolfs, A., and Luo, J. (2012). Expression patterns of ADAMs in the developing chicken lens. J. Mol. Histol. *43*, 121–135.

43. Bao, Z.Z., and Jin, Z. (2006). Sema3D and Sema7A have distinct expression patterns in chick embryonic development. Dev. Dyn. *235*, 2282–2289.

44. Lwigale, P.Y., and Bronner-Fraser, M. (2007). Lens-derived Semaphorin3A regulates sensory innervation of the cornea. Dev. Biol. *306*, 750–759.

45. Latimer, A.J., and Jessen, J.R. (2008). *Hgf/c-met* expression and functional analysis during zebrafish embryogenesis. Dev. Dyn. *237*, 3904–3915.

46. Choi, J., Park, S.Y., and Joo, C.-K. (2004). Hepatocyte growth factor induces proliferation of lens epithelial cells through activation of ERK1/2 and JNK/SAPK. Invest. Ophthalmol. Vis. Sci. *45*, 2696–2704.

47. Collinson, J.M., Quinn, J.C., Buchanan, M.A., Kaufman, M.H., Wedden, S.E., West, J.D., and Hill, R.E. (2001). Primary defects in the lens underlie complex anterior segment abnormalities of the *Pax6* heterozygous eye. Proc. Natl. Acad. Sci. USA *98*, 9688–9693.

48. Mort, R.L., Bentley, A.J., Martin, F.L., Collinson, J.M., Douvaras, P., Hill, R.E., Morley, S.D., Fullwood, N.J., and West, J.D. (2011). Effects of aberrant Pax6 gene dosage on mouse corneal pathophysiology and corneal epithelial homeostasis. PLoS ONE *6*, e28895.

49. He, F., and Jacobson, A. (2015). Nonsense-mediated mRNA decay: degradation of defective transcripts is only part of the story. Annu. Rev. Genet. *49*, 339–366.

50. Roy, B., Friesen, W.J., Tomizawa, Y., Leszyk, J.D., Zhuo, J., Johnson, B., Dakka, J., Trotta, C.R., Xue, X., Mutyam, V., et al. (2016). Ataluren stimulates ribosomal selection of near-cognate tRNAs to promote nonsense suppression. Proc. Natl. Acad. Sci. USA *113*, 12508–12513.

51. Mendell, J.T., and Dietz, H.C. (2001). When the message goes awry: disease-producing mutations that influence mRNA content and performance. Cell *107*, 411–414.

52. Collinson, J.M., Hill, R.E., and West, J.D. (2000). Different roles for Pax6 in the optic vesicle and facial epithelium mediate early morphogenesis of the murine eye. Development *127*, 945–956.